THE JOURNAL OF BIOLOGICAL CHEMISTRY VOL. 284, NO. 9, pp. 5836–5844, February 27, 2009
Printed in the U.S.A.

Structural Basis of Focal Adhesion Localization of LIM-only Adaptor PINCH by Integrin-linked Kinase*[S]

Received for publication, July 11, 2008, and in revised form, December 11, 2008 Published, JBC Papers in Press, December 30, 2008, DOI 10.1074/jbc.M805319200

Yanwu Yang[‡§1], Xiaoxia Wang[‡1], Cheryl A. Hawkins[¶], Kan Chen[‖], Julia Vaynberg[‡], Xian Mao[**], Yizeng Tu[‖], Xiaobing Zuo[‡‡], Jinbu Wang[‡‡], Yun-xing Wang[‡‡], Chuanyue Wu[‖], Nico Tjandra[¶], and Jun Qin[‡§2]**

*From the [‡]Department of Molecular Cardiology, Lerner Research Institute, The Cleveland Clinic, Cleveland, Ohio 44195, the [§]Department of Biochemistry, Case Western Reserve University, Cleveland, Ohio 44102, the [¶]Laboratory of Molecular Biophysics, NHLBI, National Institutes of Health, Bethesda, Maryland 20892, the [‖]Department of Pathology, University of Pittsburgh, Pittsburgh, Pennsylvania 15261, the [‡‡]Protein Nucleic Acid Interaction Section, Structural Biophysics Laboratory, NCI, National Institutes of Health, Frederick, Maryland 21702, and the **Cleveland Center for Structural Biology, Cleveland, Ohio 44102*

The LIM-only adaptor PINCH (the particularly interesting cysteine- and histidine-rich protein) plays a pivotal role in the assembly of focal adhesions (FAs), supramolecular complexes that transmit mechanical and biochemical information between extracellular matrix and actin cytoskeleton, regulating diverse cell adhesive processes such as cell migration, cell spreading, and survival. A key step for the PINCH function is its localization to FAs, which depends critically on the tight binding of PINCH to integrin-linked kinase (ILK). Here we report the solution NMR structure of the core ILK·PINCH complex (28 kDa, $K_D \sim 68$ nM) involving the N-terminal ankyrin repeat domain (ARD) of ILK and the first LIM domain (LIM1) of PINCH. We show that the ILK ARD exhibits five sequentially stacked ankyrin repeat units, which provide a large concave surface to grip the two contiguous zinc fingers of the PINCH LIM1. The highly electrostatic interface is evolutionally conserved but differs drastically from those of known ARD and LIM bound to other types of protein domains. Consistently mutation of a hot spot in LIM1, which is not conserved in other LIM domains, disrupted the PINCH binding to ILK and abolished the PINCH targeting to FAs. These data provide atomic insight into a novel modular recognition and demonstrate how PINCH is specifically recruited by ILK to mediate the FA assembly and cell-extracellular matrix communication.

Cell-extracellular matrix (ECM)[3] adhesion, migration, and survival are essential for the development and maintenance of tissues and organs in living organisms. They are mediated by integrin transmembrane receptors, which function by adhering to ECM proteins via their large extracellular domains while connecting to the actin cytoskeleton via their small cytoplasmic tails (20–70 residues) (1). The integrin-actin connection supports strong cell-ECM adhesion, and its alteration leads to dynamic cell shape change, migration, and survival (2). The molecular details of such connection, however, are highly complex, involving a large protein complex network called focal adhesions (FAs) (3, 4).

Integrin-linked kinase (ILK) is a 50-kDa FA protein that contains an N-terminal ankyrin repeat domain (ARD), a middle pleckstrin homology domain, and a C-terminal kinase domain. Originally discovered as an integrin β cytoplasmic tail-binding protein (5), ILK has been established as a major regulator that controls the complex FA assembly and transmits many cell adhesive signals between integrins and actin (6–8). Soon after the discovery of ILK, Tu *et al.* (9) identified an ILK binding partner called PINCH that contains five LIM domains. Extensive studies have shown that the PINCH binding to ILK is essential for triggering the FA assembly and for relaying diverse mechanical and biochemical signals between ECM and the actin cytoskeleton (9–11). Consistent with the importance of the ILK/PINCH association in almost all cellular behavior and fate, ablation of either ILK (12) or PINCH in mice is embryonically lethal (13, 14). PINCH also has a highly homologous isoform called PINCH-2. However, although complementary to PINCH in many cellular behaviors (for reviews, see Refs. 8 and 15), PINCH-2 appears to be involved at the later stage of development (16), and thus its ablation in mice is not embryonically lethal (17). At the clinical level, dysregulation of the ILK/PINCH interaction has been implicated in the development of numerous human disorders such as cancer (6, 18) and heart diseases (19, 20). A Phase I clinical trial is ongoing on a drug called thymosin β-4 (RegeneRx) that appears to specifically tar-

* This work was supported, in whole or in part, by National Institutes of Health Grants HL58758 and GM62823 (to J. Q.) and DK54639 and GM65188 (to C. W.) and by the National Institutes of Health intramural research program of the NHLBI (to N. T.) and NCI (to Y.-X. W.). This work was also supported by American Heart Association Grant 0530067N (to Y. Y.). The costs of publication of this article were defrayed in part by the payment of page charges. This article must therefore be hereby marked "*advertisement*" in accordance with 18 U.S.C. Section 1734 solely to indicate this fact.

[S] The on-line version of this article (available at http://www.jbc.org) contains supplemental Figs. S1–S3.

The atomic coordinates and structure factors (code 2kbx) have been deposited in the Protein Data Bank, Research Collaboratory for Structural Bioinformatics, Rutgers University, New Brunswick, NJ (http://www.rcsb.org/).

[1] Both authors made equal contributions to this work.

[2] To whom correspondence should be addressed: Dept. of Molecular Cardiology, NB20, Lerner Research Inst., Cleveland Clinic, 9500 Euclid Ave., Cleveland, OH 44195. Tel.: 216-444-5392; Fax: 216-445-1466; E-mail: qinj@ccf.org.

[3] The abbreviations used are: ECM, extracellular matrix; NMR, nuclear magnetic resonance; NOE, nuclear Overhauser effect; ANK, ankyrin repeat; ILK, integrin-linked kinase; PINCH, the particularly interesting cysteine- and histidine-rich protein; FA, focal adhesion; ARD, ankyrin repeat domain; GFP, green fluorescent protein; MTSSL, (1-oxyl-2,2,5,5-tetramethylpyrroline-3-methyl)methanethiosulfonate; D_a, alignment tensor; WT, wild type.

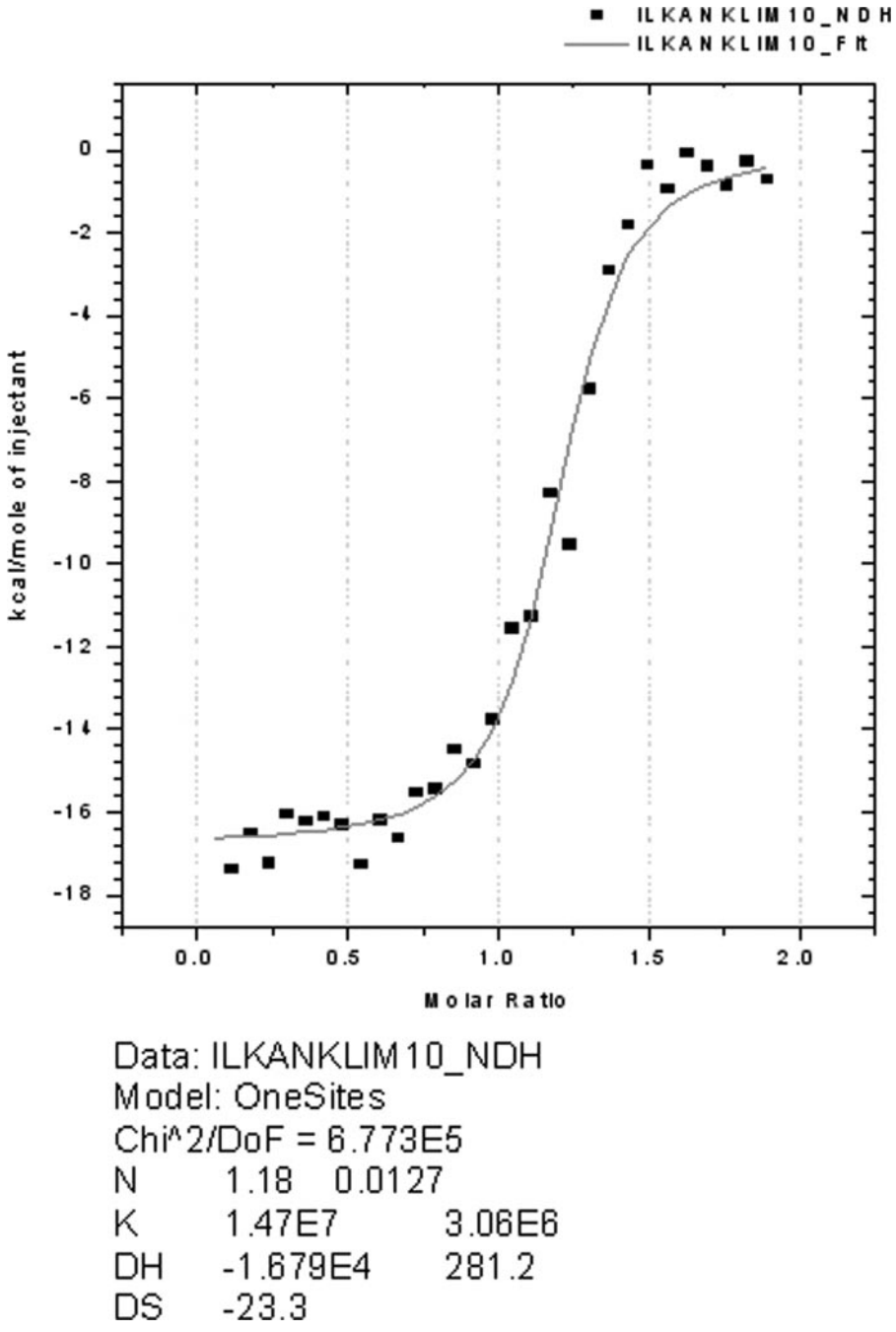

FIGURE 1. **ILK and PINCH form a tight complex.** Isothermal titration calorimetry measurement of PINCH LIM1 binding to ILK ARD at 27 °C, pH 7.0 is shown. The fitting of the curve yielded a K_D of 68 nM with ΔH (*DH*) = −16.8 kcal/mol and ΔS (*DS*) = −23 cal/mol K. *DoF*, degrees of freedom.

get ILK/PINCH for treating myocardial infarction, a major heart failure disorder (19).

Despite the cellular, physiological, and pathological importance of the ILK/PINCH interaction, the structural basis for how exactly PINCH binds to ILK has not been well understood. Previous biochemical/structural analyses have indicated that ILK utilizes its N-terminal ARD to recognize the LIM1 domain of PINCH, and such binding may promote the targeting of PINCH to FAs (9, 21). However, the precise atomic basis for such targeting process is elusive. No structure of any ARD·LIM complex has been reported. Using a combination of NMR-based techniques, we have solved the solution structure of the ILK ARD·PINCH LIM1 complex that revealed an interface that is distinct from other ARD and LIM bound to non-ARD/LIM domains. Structure-based mutation of a hot spot in PINCH LIM1, which is not conserved in other LIM domains, abolished the PINCH binding to ILK and its localization to FAs. These results not only reveal a unique LIM/ARD recognition mode but also provide a definitive functional basis for how PINCH is recruited by ILK to focal adhesion site, a major step toward the dynamic cell adhesion and migration processes.

EXPERIMENTAL PROCEDURES

DNA Constructs, Protein Expression, and Protein Purification—Initial subcloning, expression, and purification of the ILK ARD and the PINCH-1 LIM1 were described previously (21). Additional constructs were made including residues 1–171 of human ILK cloned into pTYB11 (New England Biolabs) and into pGEX-5X-3 (GE Healthcare), respectively. The former construct required no protease digestion because the fusion was chitin that could be cleaved by dithiothreitol thus eliminating the heterogeneity problem often caused by protease digestion using the pGEX construct. The ILK-(1–171) using pTYB11 construct was purified following the manufacturer's instructions (New England Biolabs). The GFP-PINCH-1 mutants for transfection experiments were made as described before (10). To prepare ^{15}N- and/or ^{13}C-labeled proteins, cells were grown in M9 minimal medium containing 1.1 g liter^{-1} [^{15}N]NH_4Cl and/or 3.3 g liter^{-1} [^{13}C]glucose. To prepare partially deuterated samples, cells were grown in minimal medium containing 70–90% ^2H_2O, but the growth rate for cell culture was slower, and thus the induction time for the protein expression was usually 2 times longer than for the undeuterated sample. Because of a precipitation problem that occurs within a week or two, many samples had to be made for the completion of all NMR experiments as required for the total structure determination. The following six different sets of samples ranging between 0.5 and 0.8 mM were made for various NMR experiments in 25 mM NaH_2PO_4, 5 mM NaCl, and 0.1–1 mM tris(2-carboxyethyl)phos-

phine, pH = 7.0 buffer (note that some samples had to be made several times because of the precipitation problem within a week or two for completion of the NMR experiments): (i) $^{15}N/^{13}C$-labeled ILK ARD bound to unlabeled LIM1, (ii) ^{15}N-, ^{13}C-, 70% ^{2}H-labeled ILK ARD bound to unlabeled LIM1, (iii) ^{15}N-labeled ILK ARD bound to unlabeled LIM1, (iv) $^{15}N/^{13}C/^{2}H$-labeled LIM1 bound to the unlabeled ILK ARD, (v) $^{15}N/^{13}C$-labeled LIM1 bound to unlabeled ILK ARD, and (vi) ^{15}N-labeled LIM1 bound to unlabeled ILK ARD. All the complex samples were purified through an S75 gel filtration column at the final stage and concentrated for NMR experiments.

Isothermal Calorimetry Measurements—Isothermal titration calorimetry was performed using a VP-ITC instrument (Microcal, Inc.). The PINCH LIM1 was dialyzed and diluted in 5 mM NaCl and 25 mM sodium phosphate, pH 7.0, to a final concentration of 6 μM. ILK ARD was prepared in the same buffer to 0.1 mM. Titrations consisted of 30 injections each; the final ratio of PINCH LIM1/ILK ARD was ~1.8 at the end of titrations. The titration curves were fitted, and thermodynamic parameters were calculated using Origin software (Microcal, Inc.).

NMR Spectroscopy—All heteronuclear NMR experiments used in the structure determination were reviewed in Ref. 22. All NMR spectra were obtained at 25 °C on a Varian Inova 600-MHz spectrometer and Bruker Avance 800 equipped with a triple resonance probe or 900-MHz spectrometer equipped with a cryogenic triple resonance probe. For resonance assignments of the bound ILK ARD or LIM1, the following triple resonance spectra of HNHA, HNCO, HNCACB, CBCACONH, CCONH, H(CCO)NH, and HCCH total correlation spectroscopy were analyzed in conjunction with three-dimensional $^{15}N/^{13}C$-edited NOE experiments. $^{1}D_{NH}$ residual dipolar couplings were measured using in-phase antiphase experiments (23) by adding roughly 12 mg/ml phage pf1 into the ^{15}N-labeled ILK ARD/unlabeled LIM1 sample or vice versa. Note that achieving exactly equal phage concentrations for the two complimentary samples was impossible. Fortunately the difference in phage concentration will only lead to an overall scaling in the dipolar coupling in the dipolars, thus magnitude of the alignment tensor (D_a). The two sets of dipolar couplings were normalized to give two different D_a values based on the distribution of the observed dipolar couplings. The direction of the alignment tensor and its rhombicity remain the same for both samples. Only dipolar couplings for those resonances that are not overlapping and not experiencing broadening due to ^{1}H-^{1}H long range dipolar couplings were included in the structure calculations (86 for the ILK ARD and 23 for the PINCH LIM1). NOE distance restraints for structure calculations were obtained from three-dimensional ^{15}N-edited and $^{15}N/^{13}C$-edited three-dimensional NOE spectroscopy spectra (mixing time, 150 ms). $^{15}N/^{13}C$-edited ^{15}N-, ^{13}C-filtered three-dimensional NOE spectroscopy (mixing time, 150 ms) was performed to examine the intermolecular NOEs, but because of the highly electrostatic nature of the interaction and the relatively large size of the complex, no intermolecular NOEs were observed. We then prepared 100% deuterated and uniformly ^{15}N-labeled ILK ARD in complex with unlabeled LIM1 and collected high sensitivity ^{15}N-edited NOE spectroscopy spectra on a 900-MHz spectrometer (two mixing times of 300 and 400 ms). A cluster of four intermolecular NOEs (ARD Arg-65 NH/LIM1 Leu-66 $C_{\delta2}H_3$, ARD Gly-66 NH/LIM1 Leu-66 $C_{\delta2}H_3$, ARD Thr-67 NH/LIM1 Leu-66 $C_{\delta2}H_3$, and ARD Asp-68 NH/LIM1 Leu-66 $C_{\delta2}H_3$) were observed. These intermolecular NOEs were further confirmed in three-dimensional ^{15}N- and three-dimensional $^{15}N/^{13}C$-edited NOE spectroscopy. The latter also led to the assignment of three additional NOEs: ARD Arg-66 NH/LIM1 $C_{\delta1}H_3$ NOEs, ARD Gly-66 Hα/LIM1 Leu-66 $C_{\delta2}H_3$, and ARD Trp-110 NϵH/LIM1 Ala-39 $C_{\beta}H_3$.

TABLE 1

Structural statistics for the solution structure of the ILK·PINCH complex

The statistics were performed using the 20 conformers with the lowest overall energies.

	r.m.s. deviations	
	20 lowest energy conformers	Lowest energy
Restraints		
Distances (Å) (3485) conformer		
Intraresidue $\|i-j\| = 0$ (1301)	0.030 ± 0.005	0.025
Sequential $\|i-j\| = 1$ (1046)	0.095 ± 0.002	0.090
Short range $\|i-j\| \leq 5$ (676)	0.10 ± 0.012	0.093
Long range $\|i-j\| \geq 5$ (421)	0.079 ± 0.004	0.068
Hydrogen bonds (Å) (329)	0.19 ± 0.07	0.11
Dihedrals (°) (368)	2.06 ± 0.22	1.58
Residual dipolar couplings (Hz) (109)		
$^{1}D_{NH}$ (ILK) (86)	1.49 ± 0.17	1.22
$^{1}D_{NH}$ (LIM) (23)	1.32 ± 0.23	1.07
Deviations from idealized covalent geometry		
Bonds (Å) (3790)	0.01 ± 0.0002	0.009
Angles (°) (6808)	1.4 ± 0.05	1.3
Impropers (°) (2040)	1.1 ± 0.03	1.1
Structure quality		
Lennard-Jones[a] potential energy (kcal/mol)	−643 ± 24	−671
Ramachandran plot analysis (%)		
All residues		
Most favored region	70.6 ± 1.4	73.5
Allowed region	22.8 ± 1.5	19.9
Generously allowed region	4.8 ± 1.1	3.8
Residues ILK 2–154 and LIM 8–67		
Most favored region	75.5 ± 1.4	77.9
Allowed region	19.7 ± 1.2	17.9
Generously allowed region	3.5 ± 0.7	2.6
Coordinate precision[b] (Å)		
Residues ILK 2–154 and LIM 8–67		
Backbone (N, Cα, C′, O)	1.18 ± 0.26	
All non-hydrogen atoms	1.64 ± 0.22	
Residues ILK 2–154		
Backbone (N, Cα, C′, O)	0.95 ± 0.12	
All non-hydrogen atoms	1.49 ± 0.12	
Residues LIM 8–67		
Backbone (N, Cα, C′, O)	0.91 ± 0.25	
All non-hydrogen atoms	1.37 ± 0.21	

[a] The Lennard-Jones van der Waals energy was calculated with the CHARMM PARAM19/20 parameters and was not included in structure calculation.

[b] The root mean square (r.m.s.) deviation is reported between the 20 conformers and the mean coordinates.

Paramagnetic Spin Labeling Experiment—The cysteine-specific spin label (1-oxyl-2,2,5,5-tetramethylpyrroline-3-methyl-)methanethiosulfonate (MTSSL) was purchased from Sigma. MTSSL was attached to the C-terminal Cys of purified LIM1-(1–70) where the residue 70 is Cys. There is no other free Cys in the construct. The preparation of the MTSSL-labeled LIM1 was as follows: 0.4 mM LIM1 and a 10-fold excess of MTSSL were mixed and stirred for 12 h in a 4:1 (v/v) solution of 25 mM sodium phosphate buffer, pH 7.0, and 10 mM NaCl and acetonitrile. Spin-labeled LIM1 was buffer-exchanged using a p10 column in the buffer containing no acetonitrile, and the final sample was confirmed by mass spectroscopy. The sample was further checked by one-dimensional ^{1}H NMR spectroscopy,

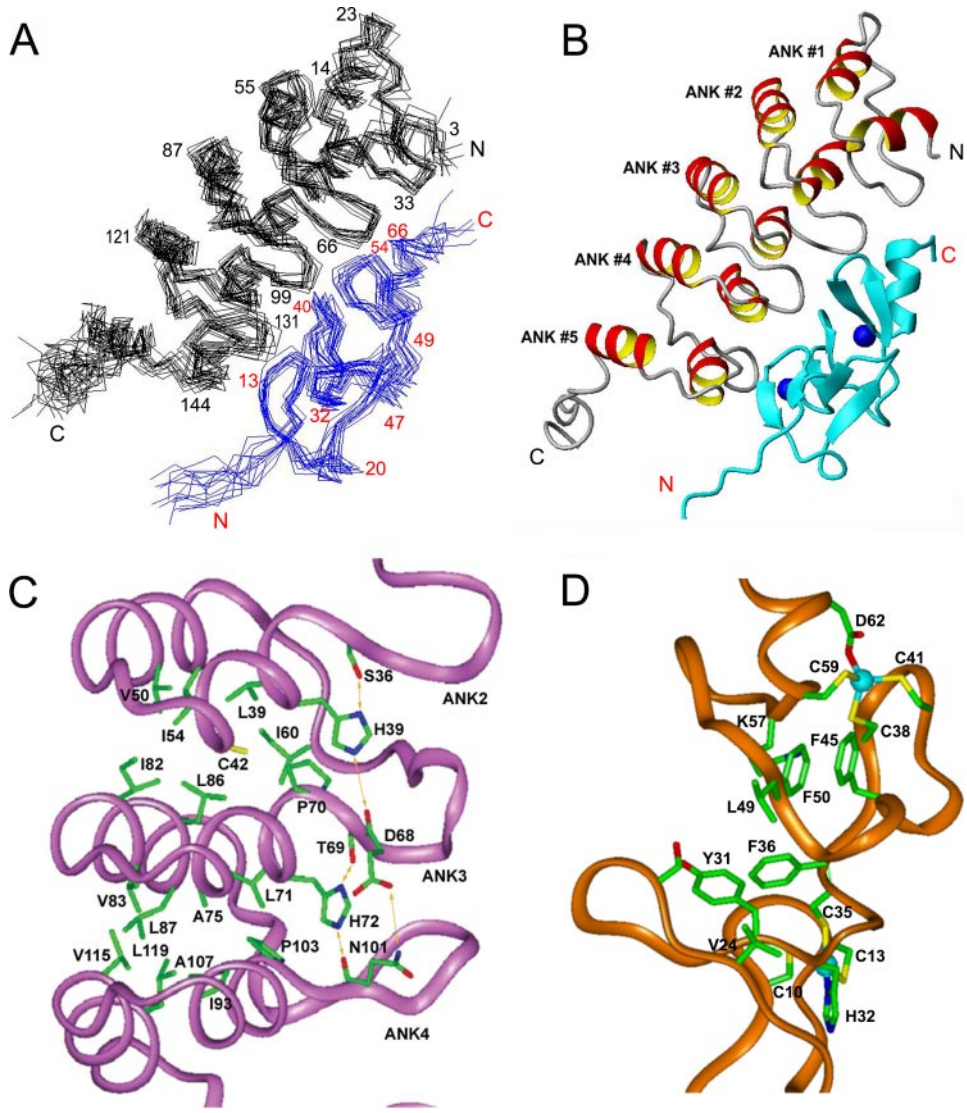

FIGURE 2. **Structure of the ILK/PINCH-1 complex.** *A*, backbone superposition of the 20 lowest energy structures for ILK ARD·PINCH-1 LIM1 complex. ILK ARD residues are labeled in *black*, and PINCH LIM1 residues are labeled in *red*. *B*, ribbon diagram of ILK ARD·PINCH-1 LIM1 complex. Notice that the five ANK units in ILK are labeled; they sequentially stack into a cupped hand shape. The two spheres in the PINCH LIM1 (*blue*) denote two zinc atoms. *C*, the zoomed region of the ARD showing the characteristic patterns of hydrophobic and hydrophilic interactions, *i.e.* the hydrophobic interactions are clustered between helices of the ANK units, whereas the hydrophilic interactions are mediated by hairpin loops. The hydrogen bond network between the hairpin loops is highlighted by *solid lines*. *D*, the central hydrophobic core linking zinc finger 1 and zinc finger 2 of PINCH LIM1. The side chains in the core are shown in *sticks* (*green*). The side chains of zinc (*cyan sphere*)-coordinating residues are also shown in *sticks*. Zinc-coordinating residues were deduced based on their geometric positions in structures calculated without zinc and were introduced to coordinate to zinc during the final stage of the structure calculations.

and the protein was folded with significant line broadening due to paramagnetic spin label as compared with non-spin-labeled LIM1. 0.3 mM spin-labeled LIM1 was mixed with the ^{15}N-labeled ILK ARD at a 1.3:1 ratio, and the heteronuclear single quantum correlation of the free ILK ARD and the mixture was collected for comparison.

Structure Calculations—The structures of bound forms of ILK ARD and PINCH LIM1 domains were calculated separately using protocols described previously (24). The ^{1}H(N)/^{15}N chemical shift mapping data were transformed into a set of ambiguous, intermolecular distance restraints according to the two criteria defined in Ref. 25, *i.e.* the significant chemical shift perturbation of the residues and their surface accessibility in the individual subunits. The dipolar couplings were incorporated into structure calculation as described previously (25, 26). The alignment tensor was initially estimated using the histogram approach (27) and later optimized by the grid search method as described previously (28). Because the dipolar couplings for the ILK ARD and the PINCH LIM1 were acquired with different samples the magnitude of their D_a was optimized separately while keeping the rhombicity and the alignment tensor direction the same. The final optimized D_a values are 11.8 and 8.2 Hz for the ILK ARD and the PINCH LIM1, respectively. The optimized rhombicity used was 0.48. The complex structure was obtained by simulated annealing of the ILK ARD and the PINCH LIM1 structures with slowly increasing forces on the intermolecular NOEs, the chemical shift-based intermolecular ambiguous distances, the van der Waals repulsion, and the dipolar coupling restraints. All structures satisfying the experimental restraints (*i.e.* both the ambiguous intermolecular distance restraints and the dipolar couplings) converge to a single cluster. In the next iteration the ambiguity in the chemical shift-based intermolecular restraints was reduced by examining the resulting structures so that residues that are clearly outside the interaction clusters were eliminated, and a total of 200 final structures were calculated from which 20 with the lowest energies were chosen for analysis and deposited in the Protein Data Bank (code 2kbx).

DNA Transfection, Immunoprecipitation, and Immunofluorescence Staining—Human SK-LMS-1 cells were transfected with DNA vectors encoding GFP or GFP-tagged wild type and mutant forms of PINCH-1 using Lipofectamine 2000. One day after the transfection, the cells were analyzed by immunoprecipitation and immunofluorescence staining. For immunoprecipitation, the cells were lysed with 1% Triton X-100 in 50 mM Tris-HCl, pH 7.4 containing 150 mM NaCl, 10 mM $Na_4P_2O_7$, 2 mM Na_3VO_4, 100 mM NaF, and protease inhibitors. The lysates (350 μg) were mixed with 2 μl of rabbit anti-GFP antiserum (Clontech). The anti-GFP immune complexes were precipitated with 20 μl of protein A/G plus-agarose beads (Santa Cruz

Biotechnology). After washing, the precipitated proteins were released from the beads by boiling in 30 μl of SDS-PAGE sample buffer for 5 min and analyzed by Western blotting with a polyclonal anti-GFP antibody (Santa Cruz Biotechnology) or a monoclonal anti-ILK antibody (clone 65.1).

RESULTS

The Structure of the ILK ARD/PINCH LIM1 Complex—To understand the nature of the ILK/PINCH interaction, we first decided to measure the binding affinity of the complex by performing the isothermal titration calorimetry experiment. Fig. 1 shows the binding profile of the ILK ARD to PINCH LIM1. Consistent with the large chemical shift changes upon the ILK ARD/PINCH LIM1 interaction (supplemental Fig. S1, a and b), the isothermal titration calorimetry experiment revealed a strong binding affinity at K_D ~68 nM (Fig. 1). The complex was found to be more stable at low salt concentration, although its heteronuclear single quantum correlation perturbation pattern at low salt (supplemental Fig. S1a) is the same as that at high salt condition as shown previously (21). The stable interaction at lower ionic strength and the enthalpy-driven nature of the binding (Fig. 1) are consistent with the highly electrostatic interface of the structure as revealed at a later stage of the study. It is also consistent with the fact that only a very limited number of intermolecular NOEs were obtained between the two subunits. The structure of the complex was thus calculated by using residual dipolar couplings and ambiguous chemical shift mapping-based distance constraints (25) and intermolecular NOEs. Such a protocol successfully led to a well converged structure, which was independently confirmed by multiple additional experiments (see below). Table 1 summarizes the structural statistics for the 20 final calculated structures with the lowest energies. The root mean square deviations for the structures are 1.18 Å for the backbone and 1.64 Å for all heavy atoms (also see Fig. 2*A*).

Examination of the structure revealed that the bound ILK ARD (residues 2–154) is quite elongated, containing five sequentially stacked ankyrin repeats (ANKs) (Fig. 2*B*). Each ANK adopts the typical ANK fold (29) with a conserved helix-turn-helix conformation preceded by a β-hairpin-like loop with the exception of the first ANK (residues 2–20). The first ANK unit was not recognized previously because of little sequence homology to the consensus ANK sequence, but its ANK fold was clear in our NOE analysis and structure calculations (Fig. 2*B*). The stacking of the adjacent ANKs is mediated by highly conserved hydrophobic interactions between the helices of the helix-turn-helix motifs and hydrophilic interactions between the hairpin-like loops (Fig. 2*C*). The hydrophilic interactions involve a series of side-chain and backbone hydrogen bonds and/or salt bridges (Fig. 2*C*). The overall structure of the ILK ARD is like a cupped hand with hairpin-like loops protruding to one side of the ARD structure (Fig. 2*B*). Such a sequential folding pattern emphasizes the importance of every ANK unit, especially the middle units because they contact the ANK units both before and after them. Deletion of any of these ANK units, especially the middle units, would disrupt the integrity of the ARD folding (29) (supplemental Fig. S2) and its function (30). The bound LIM1 (residues 8–67) adopts the characteristic

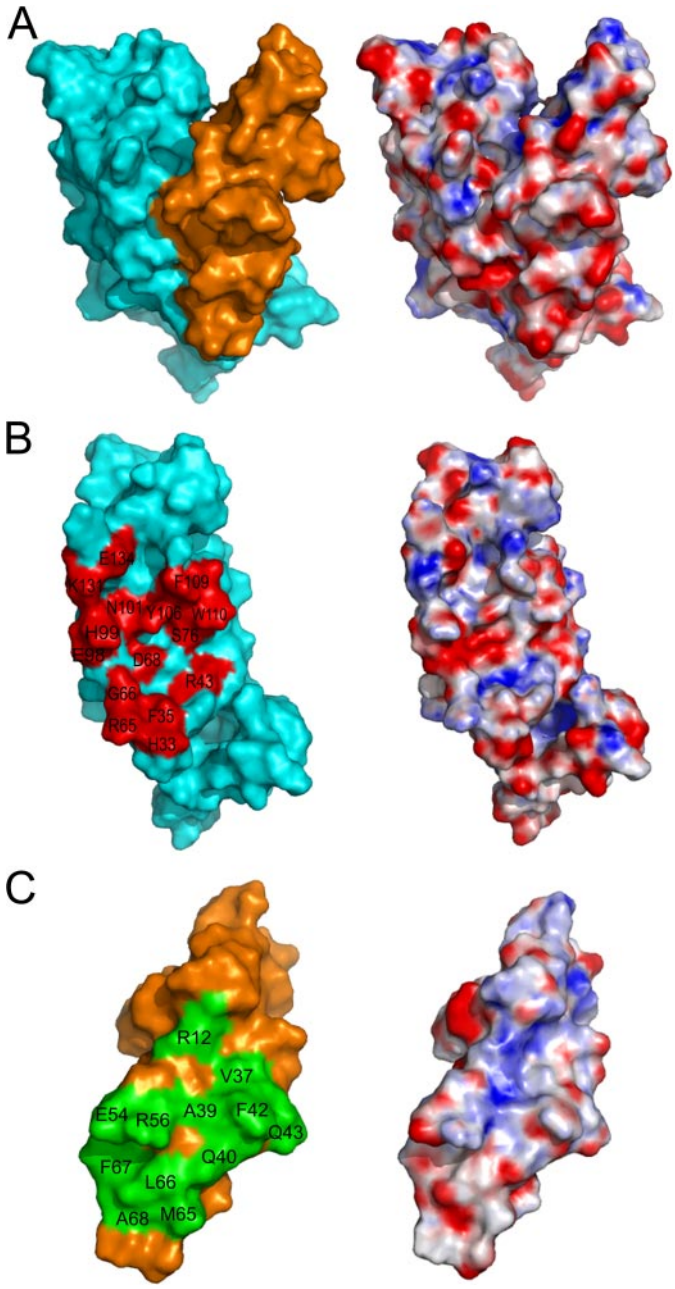

FIGURE 3. **Structural features of ILK ARD·PINCH LIM1 complex.** *A*, overall surface plot of the ILK ARD (*light blue*)·PINCH LIM1 (*light brown*) complex (*left*). The surface features are shown on the *right*. *Red*, negative charge; *blue*, positive charge; *white*, hydrophobic. The surface was generated by GRASP. *B*, surface of the bound ILK ARD with the LIM1 binding site colored in *red* (*left panel*) and electrostatic feature shown in the *right panel* in the same view. *C*, surface of the bound PINCH LIM1 with the ARD binding site colored in *green* (*left panel*) and electrostatic feature shown in the *right panel* in the same view.

double zinc finger structure with four antiparallel β-sheets followed by a short helix (Fig. 2*B*). The overall shape of the bound LIM1 is also elongated (Fig. 2*D*); this is similar to but not identical to the previously reported unbound LIM1 (21), indicating some binding-induced conformational change. The two zinc fingers are linked by a central hydrophobic core involving Val-24, Tyr-31, Phe-36, Pro-46, Leu-49, Phe-50, and the hydrophobic part of Lys-57 (Fig. 2*D*).

The surface presentation of the whole complex is shown in Fig. 3*A*, which exhibits a head-to-tail packing. Such packing is

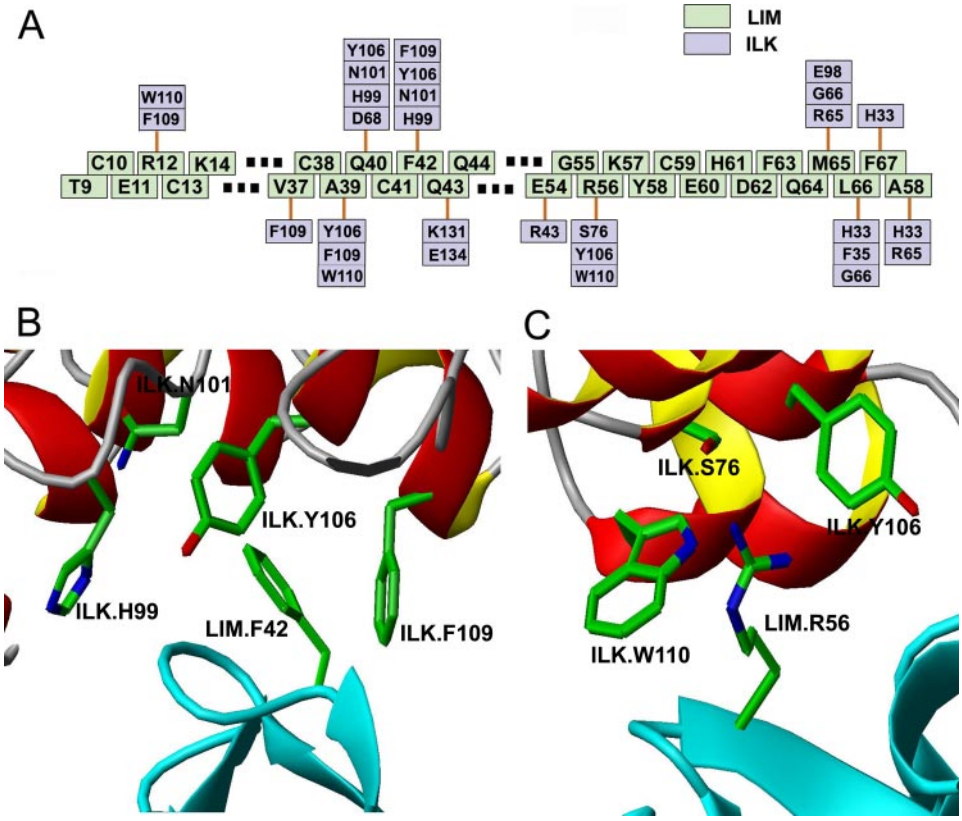

FIGURE 4. **Summary of the ILK/PINCH interface.** *A*, a diagram summarizing the ILK ARD/PINCH LIM1 interactions. Three segments in PINCH LIM1 are shown that are involved in interacting with ILK ARD. Specific residues in PINCH LIM1 that have potential contacts based on the ensemble structures with ILK ARD residues are linked by the *solid lines*. *B* and *C*, zoomed views of certain interface regions suggesting multiple contacts involving ILK ARD and PINCH LIM1. Note that the *blue sticks* indicate nitrogen atoms and that the *red sticks* indicate oxygen atoms.

consistent with the paramagnetic spin labeling experiment in which adding a bulky spin label (MTSSL) to the C-terminal Cys of LIM1 prevented the LIM1 binding to the ILK ARD (supplemental Fig. S3).

Distinct Interaction Features of the ILK ARD·PINCH LIM1 Complex and Comparison with Other ARD or LIM Complexes—Although the structures of the bound the ILK ARD and PINCH LIM1 adopt conserved folding patterns, the binding interface appears to be quite distinct with highly electrostatic nature (Fig. 3, *B* and *C*). The interface (~1800 Å) is larger than the observed average value of 1600 Å for the protein complex interface (31), which is consistent with the tight ILK/PINCH binding (K_D ~ 68 nM). The highly polar feature of the interface also explains why the binding is enthalpy-driven (Fig. 1) and why the complex is more stable at low salt condition. Fig. 4*A* summarizes the binding site information. Although the majority of the contacts are hydrophilic, a significant number of hydrophobic interactions are also present especially involving aromatic residues (Fig. 4*A*). The interactions are exemplified in Fig. 4, *B* and *C*, respectively. Characteristically many hydrophilic residues from the hairpin tips and the first α-helices of the ANK units 2–5 in the ILK ARD are involved in the binding (Fig. 5*A*). These residues form a distinct surface (Fig. 3*B*) that recognizes a complementary interface in the PINCH LIM1 (Fig. 3*C*) involving two zinc fingers and a portion of the C-terminal helix (Fig. 5*B*). The second zinc finger seems to be more important as it encompasses more than 80% of the interface. This is consistent with the previous deletion mutagenesis data, which revealed that the C-terminal region of LIM1 plays a dominant role in ILK binding (30).

Because previous studies have demonstrated that the ILK/PINCH interaction is crucial in a variety of species (for a review, see Ref. 7), we wondered whether the ILK/PINCH interface is conserved in these species. We therefore compared the three most representative sequences from human, *Drosophila*, and *Caenorhabditis elegans*, which are the most widely varied among all species (7). Fig. 5 shows that the binding interface for the ILK·PINCH complex in these species is highly conserved. Thus our data provide the definitive structural basis for understanding the essential role of the ILK/PINCH interaction in mediating cell adhesion and migration in all species.

The ILK ARD/PINCH LIM1 interface represents the first example of an interaction between the two widely distributed protein binding domains (ARD and LIM). To understand the specificity of the ILK ARD/PINCH LIM1 interaction, we compared its recognition pattern with other types of known ARD and LIM complexes. Three representative ARDs were chosen; all exhibit the cupped hand fold, but they bind to distinct targets. These ARDs include transcription regulator GABP that binds to the ETS DNA binding domain (32), tumor suppressor p16 that binds to the kinase domain of cyclin-dependent kinase Cdk6 (33), and IκBα that binds to and inhibits transcription factor NFκB (34, 35). Fig. 5*A* shows that although the binding region in the ILK ARD shares some shape-specific features with other ARDs, *e.g.* the β-hairpin like loops are involved in the interaction, the specific interface residues are drastically different. The binding mode of the PINCH LIM1 was compared with two other available LIM complex structures including the PINCH LIM4 bound to Nck-2 adaptor (24) and oncoprotein LMO4 LIM1 and LIM2 bound to nuclear adaptor Ldb1 (36). As summarized in Fig. 5*B*, the ILK binding sequence on the PINCH LIM1 is also entirely different from those for either the PINCH LIM4 or the LIMO LIM complexes. Interestingly the PINCH LIM1 and LMO4 LIM1 utilize both zinc fingers and the C-terminal helix to tightly bind to targets, although the specific binding regions and the residues involved are totally different.

PINCH Binding to ILK Is Critical for the PINCH Targeting to FAs—To functionally evaluate the mechanism of PINCH binding to ILK, we made structure-based point mutations on two interface residues, Phe-42 and Arg-56, in full-length PINCH

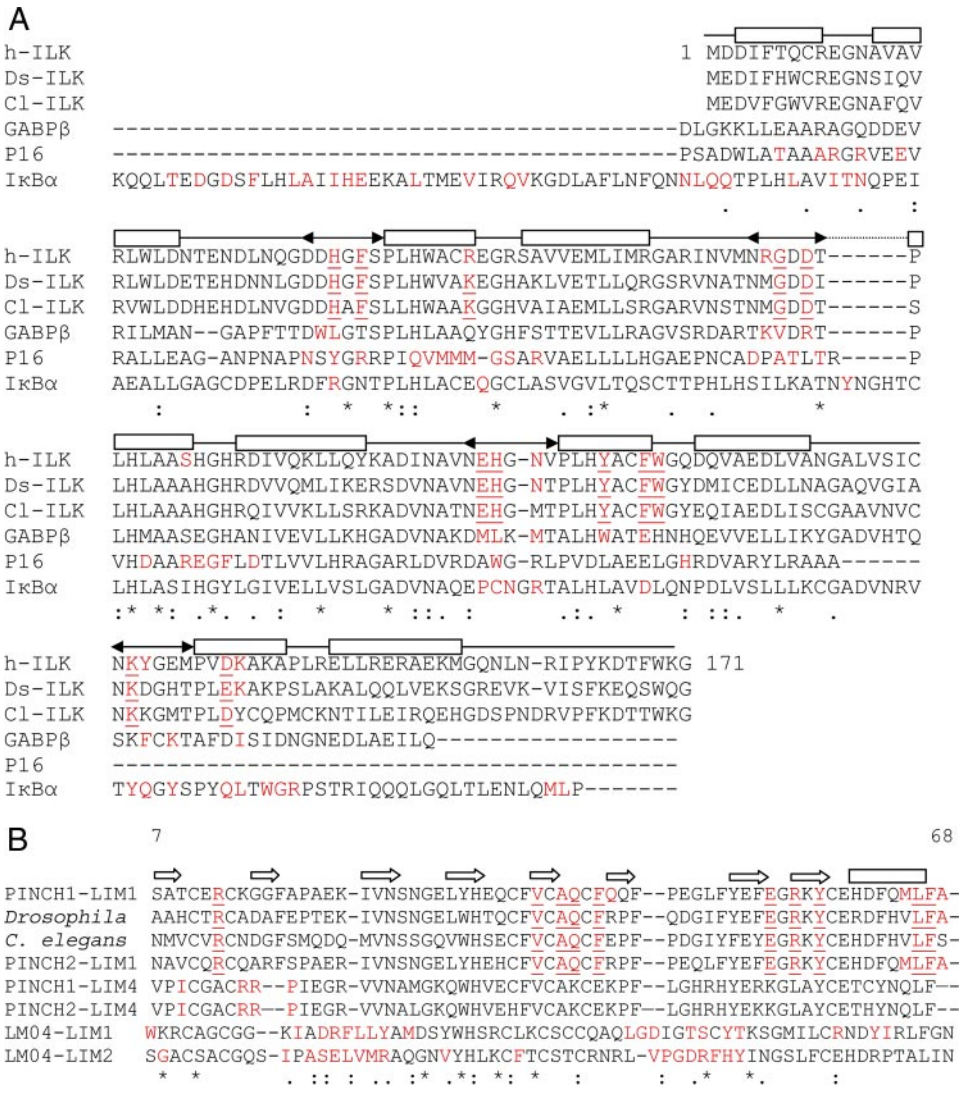

FIGURE 5. **Structural and binding features of ILK ARD and PINCH-1 LIM1.** *A*, structure-based sequence alignment of ILK ARD (human (h), *Drosophila* (*Ds*), and *C. elegans* (*Cl*)) with other representative ARDs including GABPβ, p16, and IκBα. * identical residues, : indicates very similar residues, and . indicates similar residues. Secondary structural features for ILK ARD are highlighted *above* the sequence. *Rectangles* stand for helices, and *double arrows* are for β-hairpin loops. Specific residues for all ARDs involved in binding to different targets are highlighted in *red*. Identical binding residues of ILK ARD in different species are *underlined*. *B*, alignment of PINCH LIM1 (human, *Drosophila*, and *C. elegans*) with PINCH LIM4 and other LIM domains whose interactions with other proteins have been reported. Secondary structural features are highlighted *above* the sequence. *Rectangles* stand for helices, and *arrows* are for β-strands. Specific residues for all LIMs involved in binding to targets are highlighted in *red*. Identical binding residues of PINCH LIM1 in different species are *underlined*.

(Fig. 4, *B* and *C*) into Ala, respectively. Both Phe-42 and Arg-56 are conserved in the PINCH LIM1 family members but not in other LIM domains (Fig. 5*B*). Fig. 6 shows that although both F42A and R56A have the same expression as WT PINCH (Fig. 6*A*) the F42A binding to ILK was completely lost and the R56A binding to ILK was slightly reduced (Fig. 6*B*) indicating that aromatic Phe-42-mediated hydrophobic contacts contribute substantially to the ILK/PINCH binding energy. Consistently compared with WT PINCH (Fig. 6, *C* and *D*), F42A completely failed to localize to FAs (Fig. 6, *E* and *F*), whereas R56A still had effect (Fig. 6, *G* and *H*). It has been reported previously that Q40A mutation in PINCH (11, 37) also causes defects in cell spreading, migration, and survival (11, 37). Examination of the structure revealed that Gln-40 resides in a loop between the two β-strands and that its side chain protrudes onto the surface, making multiple potential contacts with the ILK ARD (Fig. 4*A*). It is clear that replacement of Gln-40 with Ala would completely remove these contacts thereby disrupting the PINCH/ILK interaction (10) and the PINCH/ILK-mediated cell adhesion processes.

DISCUSSION

Mounting evidence has indicated that the binding of PINCH to ILK is essential for the assembly of FAs and for regulating cytoskeleton and cell adhesion (5). However, the detailed structural basis of the interaction has remained elusive. Our data now provide definitive insight into how PINCH binding to ILK promotes the localization of PINCH to cell-ECM adhesion sites. The structure also provides an important template for further investigating the ILK/PINCH-mediated supramolecular FA assembly and signaling. As shown in Fig. 3*A*, the ILK ARD and PINCH LIM1 are packed in a head-to-tail manner. The directions of the subunits in such a packing mode suggest that the rest of ILK and PINCH may be extended out. Although this model requires future investigation, it is consistent with the following facts. (i) The ILK ARD has no interaction with ILK kinase domain when the kinase domain is bound to α-parvin, another FA molecule that binds to F-actin (data not shown). (ii) The tandem PINCH LIM domains are linearly arrayed as indicated by our NMR data (21, 24). Such extended conformation may favor the docking of other proteins such as parvin, Nck-2, etc. (7) thereby facilitating the formation of supramolecular FA machinery.

From a protein recognition point of view, our structure also revealed a novel mode of modular recognition between LIM and ARD: two widely distributed protein interaction domains. We showed that such recognition is evolutionally conserved across the species supporting the essential role of the ILK/PINCH interaction in cell adhesive processes. Disruption of this interaction either by point mutation (Ref. 10 and Fig. 6) or by deletion of important binding fragments in the ILK ARD (30, 38) or in the PINCH LIM1 (30) causes a spectrum of cellular defects. On the biomedical side, our structure may help the design of specific compounds or peptide-mimetic agents for

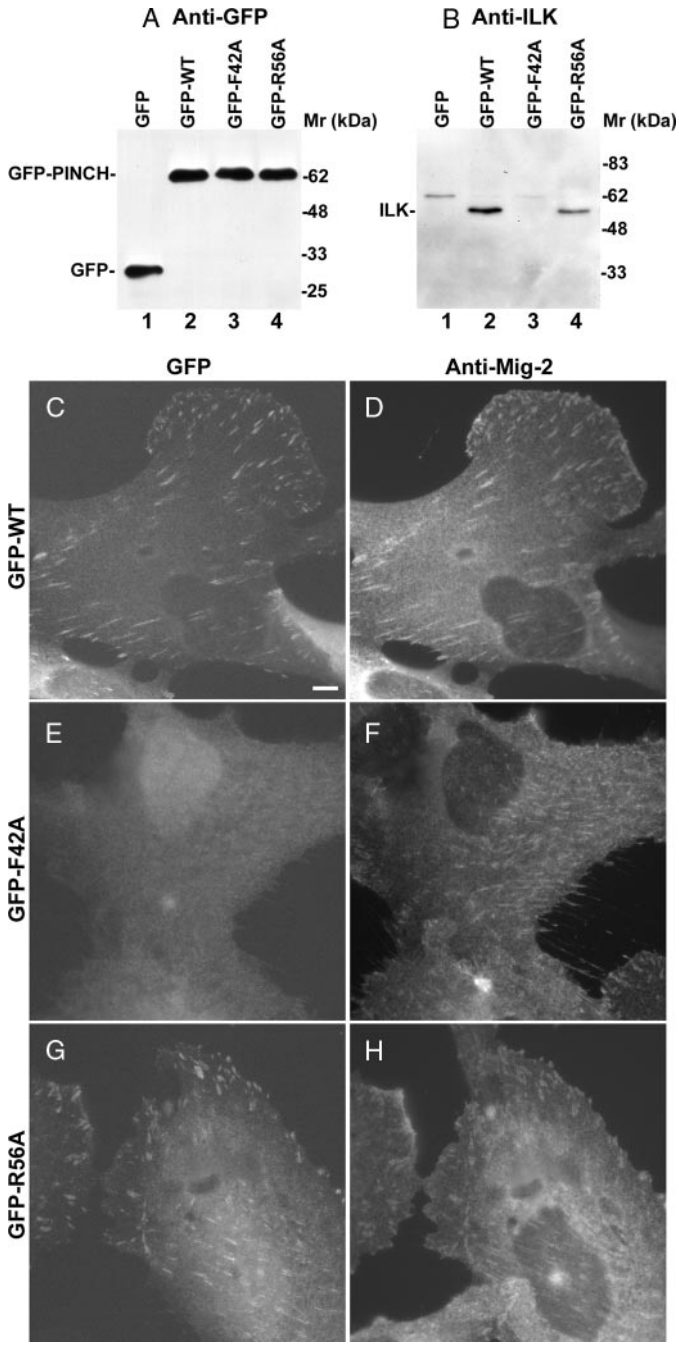

FIGURE 6. **The effect of structure-based interface mutations on PINCH/ILK interaction and the PINCH localization to FAs.** *A*, the expression levels of GFP vector alone, WT GFP-PINCH-1, F42A, and R56A. Lysates of C2C12 cells expressing GFP-tagged wild type or mutant (Phe-42 → Ala and Arg-56 → Ala) forms of PINCH were mixed with rabbit anti-GFP antibodies and measured by Western blotting. *B*, complex formation of WT PINCH and PINCH mutants with ILK. The GFP-PINCH (*lane 2*), GFP-F42A (*lane 3*), and GFP-R56A (*lane 4*) immunoprecipitates were analyzed by Western blotting with mouse monoclonal anti-ILK antibody 65.1 and horseradish peroxidase-conjugated anti-mouse IgG antibodies. *C–H*, subcellular localization. C2C12 cells transfected with expression vectors encoding GFP-WT PINCH (*C* and *D*), F42A (*E* and *F*), or R56A (*G* and *H*) were plated on fibronectin-coated coverslips and stained with a mouse monoclonal anti-Mig-2 antibody (as a marker of focal adhesions) and a Rhodamine Red™-conjugated anti-mouse IgG antibody. GFP-F42A, GFP-R56A, GFP-PINCH, and Mig-2 were visualized under a fluorescence microscope equipped with GFP (*C*, *E*, and *G*) and rhodamine (*D*, *F*, and *H*) filters. *Bar*, 10 μm.

detailed investigation and/or treatment of the ILK/PINCH-mediated diseases. Substantial elevation of ILK and/or PINCH levels has been detected in several cancers suggesting that manipulating the ILK·PINCH complex level in these cancers may be therapeutically useful (for a review, see Ref. 6). Indeed inhibition of the ILK expression and activity has been shown to suppress tumors (for a review, see Ref. 6). Increasing animal model-based evidence is also pointing to an important role of the ILK·PINCH complex in mediating heart disease, a major cause of death in humans (for a review, see Ref. 39). By examining human patient hearts with dilated cardiomyopathy, a major heart failure disease, we found that not only the individual ILK and PINCH levels but also the level of their complex was highly elevated in human failing hearts.[4] Thus, our structure may provide an important template for designing agents to further investigate heart disease and other diseases that in turn lead to more effective therapies for these diseases.

Acknowledgments—We thank F. Delaglio for nmrPipe software; D. Garrett for PIPP; and Marius Clore, Saurav Misra, Dhanuja Perera, Algirdas Velyvis, Sudhi Gupta, Asta Velyviene, Koichi Fukuda, Sujay Ithychanda, and Xiaolun Zhang for useful discussion and technical assistance.

REFERENCES

1. Hynes, R. O. (1992) *Cell* **69,** 11–25
2. Brakebusch, C., and Fassler, R. (2003) *EMBO J.* **22,** 2324–2333
3. Critchley, D. R. (2000) *Curr. Opin. Cell Biol.* **12,** 133–139
4. Geiger, B., Bershadsky, A., Pankov, R., and Yamada, K. M. (2001) *Nat. Rev. Mol. Cell Biol.* **2,** 793–805
5. Hannigan, G. E., Leung-Hagesteijn, C., Fitz-Gibbon, L., Coppolino, M. G., Radeva, G., Filmus, J., Bell, J. C., and Dedhar, S. (1996) *Nature* **379,** 91–96
6. Hannigan, G., Troussard, A. A., and Dedhar, S. (2005) *Nat. Rev. Cancer* **5,** 51–63
7. Wu, C. (2005) *Trends Cell Biol.* **15,** 460–466
8. Legate, K. R., Montanez, E., Kudlacek, O., and Fassler, R. (2006) *Nat. Rev. Mol. Cell Biol.* **7,** 20–31
9. Tu, Y., Li, F., Goicoechea, S., and Wu, C. (1999) *Mol. Cell. Biol.* **19,** 2425–2434
10. Zhang, Y., Chen, K., Tu, Y., Velyvis, A., Yang, Y., Qin, J., and Wu, C. (2002). *J. Cell Sci.* **115,** 4777–4786
11. Fukuda, T., Chen, K., Shi, X., and Wu, C. (2003) *J. Biol. Chem.* **278,** 51324–51333
12. Sakai, T., Li, S., Docheva, D., Grashoff, C., Sakai, K., Kostka, G., Braun, A., Pfeifer, A., Yurchenco, P. D., and Fassler, R. (2003) *Genes Dev.* **17,** 926–940
13. Li, S., Bordoy, R., Stanchi, F., Moser, M., Braun, A., Kudlacek, O., Wewer, U. M., Yurchenco, P. D., and Fassler, R. (2005). *J. Cell Sci.* **118,** 2913–2921
14. Liang, X., Zhou, Q., Li, X., Sun, Y., Lu, M., Dalton, N., Ross, J., Jr., and Chen, J. (2005) *Mol. Cell. Biol.* **25,** 3056–3062
15. Wu, C. (2004) *Biochim. Biophys. Acta* **1692,** 55–62
16. Braun, A., Bordoy, R., Stanchi, F., Moser, M., Kostka, G. G., Ehler, E., Brandau, O., and Fassler, R. (2003) *Exp. Cell Res.* **284,** 239–250
17. Stanchi, F., Bordoy, R., Kudlacek, O., Braun, A., Pfeifer, A., Moser, M., and Fassler, R. (2005). *J. Cell Sci.* **118,** 5899–5910
18. Huang, H. C., Hu, C. H., Tang, M. C., Wang, W. S., Chen, P. M., and Su, Y. (2007) *Oncogene* **26,** 2781–2790
19. Bock-Marquette, I., Saxena, A., White, M. D., Dimaio, J. M., and Srivastava, D. (2004) *Nature* **432,** 466–472

[4] S. Gupta and J. Qin, unpublished results.

20. Chen, H., Huang, X. N., Yan, W., Chen, K., Guo, L., Tummalapali, L., Dedhar, S., St-Arnaud, R., Wu, C., and Sepulveda, J. L. (2005) *Lab. Investig.* **85,** 1342–1356
21. Velyvis, A., Yang, Y., Wu, C., and Qin, J. (2001) *J. Biol. Chem.* **276,** 4932–4939
22. Clore, G. M., and Gronenborn, A. M. (1998) *Curr. Opin. Chem. Biol.* **2,** 564–570
23. Ottiger, M., Delaglio, F., and Bax, A. (1998) *J. Magn. Reson.* **131,** 373–378
24. Vaynberg, J., Fukuda, T., Chen, K., Vinogradova, O., Velyvis, A., Tu, Y., Ng, L., Wu, C., and Qin, J. (2005) *Mol. Cell* **17,** 513–523
25. Clore, G. M., and Schwieters, C. D. (2003) *J. Am. Chem. Soc.* **125,** 2902–2912
26. De Alba, E., and Tjandra, N. (2002) *Prog. Nucl. Magn. Reson. Spectrosc.* **40,** 175–197
27. Clore, G. M., Gronenborn, A. M., and Bax, A. (1998) *J. Magn. Reson.* **133,** 216–221
28. Clore, G. M., Gronenborn, A. M., and Tjandra, N. (1998) *J. Magn. Reson.* **131,** 159–162
29. Li, J., Mahajan, A., and Tsai, M. D. (2006). *Biochemistry* **45,** 15168–15178
30. Li, F., Zhang, Y., and Wu, C. (1999) *J. Cell Sci.* **112,** 4589–4599
31. Jones, S., and Thornton, J. M. (1996) *Proc. Natl. Acad. Sci. U. S. A.* **93,** 13–20
32. Batchelor, A. H., Piper, D. E., de la Brousse, F. C., McKnight, S. L., and Wolberger, C. (1998) *Science* **279,** 1037–1041
33. Russo, A. A., Tong, L., Lee, J. O., Jeffrey, P. D., and Pavletich, N. P. (1998) *Nature* **395,** 237–243
34. Jacobs, M. D., and Harrison, S. C. (1998) *Cell* **95,** 749–758
35. Huxford, T., Huang, D. B., Malek, S., and Ghosh, G. (1998) *Cell* **95,** 759–770
36. Deane, J. E., Mackay, J. P., Kwan, A. H., Sum, E. Y., Visvader, J. E., and Matthews, J. M. (2003) *EMBO J.* **22,** 2224–2233
37. Xu, Z., Fukuda, T., Li, Y., Zha, X., Qin, J., and Wu, C. (2005) *J. Biol. Chem.* **280,** 27631–27637
38. Nikolopoulos, S. N., and Turner, C. E. (2002) *J. Biol. Chem.* **277,** 1568–1575
39. Srivastava, D., and Yu, S. (2006) *Genes Dev.* **20,** 2327–2331